Hydrol. Earth Syst. Sci. Discuss., 10, 8117–8144, 2013
www.hydrol-earth-syst-sci-discuss.net/10/8117/2013/
doi:10.5194/hessd-10-8117-2013

Hydrology and Earth System Sciences
Open Access
Discussions

FAO-56 dual approach combined with multi-sensor remote sensing for regional evapotranspiration estimations

R. Amri[1,2], M. Zribi[1], Z. Lili-Chabaane[2], C. Szczypta[1], J. C. Calvet[3], and G. Boulet[1]

[1]CESBIO, 18 av. Edouard Belin, UMR5126, CNRS, bpi 2801, 31401 Toulouse cedex 9, France
[2]INAT, 43, Avenue Charles Nicolle 1082 -Tunis- Mahrajène, Tunisie
[3]CNRM-GAME, Météo-France, CNRS, URA1357, 42 avenue Gaspard Coriolis, Toulouse, France

Received: 21 May 2013 – Accepted: 10 June 2013 – Published: 24 June 2013

Correspondence to: M. Zribi (mehrez.zribi@cesbio.cnes.fr)

Published by Copernicus Publications on behalf of the European Geosciences Union.

Abstract

The aim of this paper is to use a dual, modified version of the FAO-56 methodology for the estimation of regional evapotranspiration. The proposed approach combines the FAO-56 technique with remote sensing. Two vegetation classes are considered in the evapotranspiration estimations. In the case of cereals, crop coefficients and cover fractions are estimated using relationships established with the Normalized Difference Vegetation Index (NDVI), retrieved from SPOT-VGT data. In order to characterize the soil, a relationship is established between evaporation and the retrieved soil moisture values, based on the ERS/WSC products developed by the University of Vienna. This approach is applied to a semi-arid region in central Tunisia (North Africa) and is validated over 1991–2007 period using simulations from the ISBA-A-gs physical SVAT model. The ISBA soil moisture outputs are validated using remotely sensed ERS/WSC products. Finally, a comparison is made between the ISBA and FAO approaches, for the same studied site.

1 Introduction

In semi-arid regions, and the Mediterranean basin in particular, agricultural productivity and water resources suffer from serious crises as a consequence of limited levels of precipitation, combined with the occurrence of long periods of drought. In this context, the accurate monitoring of vegetation cover and hydric stress can be a valuable tool, especially for those areas which rely on rainfed agriculture. A second challenge for the well-adapted management of this agriculture is to accurately determine the evapotranspiration, in order to quantify the soil water stock. In recent years, a variety of physical surface models have been proposed at regional and global scales. The most accurate of these is the SVAT (Soil – Vegetation – Atmosphere Transfer) model (Noilhan and Planton, 1989; Braud et al., 1995; Mahfouf et al., 1995; Calvet et al., 1998; Coudert et al., 2006).

HESSD
10, 8117–8144, 2013

On the other hand, the FAO-56 model is the most commonly used and practical approach for the estimation of crop water requirements and local scale evapotranspiration (Allen et al., 1998). It is estimated simply through the combination of a reference evapotranspiration value (ET_0) and crop coefficients. The dual FAO-56 approach uses two coefficients to separate the respective contributions of plant transpiration (K_{cb}) and soil evaporation (Allen et al., 2000). In recent years, various studies have attempted to combine this model with remote sensing data for operational applications. These attempts were motivated in particular by the retrieval of vegetation cover dynamics from optical satellite vegetation indexes (Purevdorj et al., 1998; Duchemin et al., 2006; Er-Raki et al., 2007). The applications of this model are related mainly to the study of irrigated areas, for the effective planning of irrigation water use. The aim of the present study was to propose the combined use of this simple tool with remote sensing, for the purposes of regional evapotranspiration estimations, without making use of complex physical surface models requiring large quantities of input data. In recent years, sustained scientific activity based on the interpretation of remotely sensed signals has made it possible to develop various methodologies for the characterization of the spatio-temporal variability of continental surface parameters (vegetation characteristics and soil moisture), on both local and global scales. In the case of vegetation cover, different indexes based on optical sensors have been proposed, for the retrieval of vegetation characteristics (leaf area index, vegetation fraction, ...). The most commonly used of these is the NDVI, which is expressed as: NDVI = (RNIR – RRED)/(RNIR + RRED), where RNIR is the near-infrared (NIR) reflectance and RRED is the red reflectance. This index is sensitive to the presence of green vegetation (Sellers, 1985) and has been used in various different studies dealing with the estimation of potential photosynthetic activity of vegetation (Deblonde et al., 1993; Myneni et al., 1995; Propastin et al., 2009; Er-Raki et al., 2010; Laurila et al., 2010). As a consequence of its formulation, the NDVI is able to robustly characterize green vegetation, despite varying atmospheric conditions in the red and NIR bands (Fraser and Kaufman, 1985; Holben et al., 1990). Several different methodologies based on the interpretation of microwave sensor data have been

HESSD
10, 8117–8144, 2013

developed for the determination of soil moisture (Jackson et al., 1996; Ulaby et al., 1996; Paloscia et al., 2008). A large number of studies have demonstrated the potential of low-resolution spaceborne (active microwave) scatterometers for land surface characterization, in particular for the estimation of soil moisture (Wagner et al., 1999; Zribi et al., 2003, 2008; Ceballos et al., 2005; Pellarin et al., 2006; Paris Anguela et al., 2008).

The aim of the present study was to adapt the FAO dual approach, combined with remotely sensed (satellite) data, for the purposes of regional evapotranspiration estimations. In Sect. 2, the studied site and the remotely sensed and ground databases are presented. In Sect. 3, the dual FAO model is introduced, and the concurrent use of remotely sensed data is discussed. In Sect. 4, the proposed approach is validated through the use of a physical SVAT model: ISBA-A-gs. Finally, the authors' conclusions are presented in Sect. 5.

2 Database and processing

2.1 Studied site

The studied site is the Kairouan plain, which is situated in central Tunisia (35°–35°45′ N; 9°30′–10°15′ E) (Fig. 1) and is characterized by a semi-arid climate (Zribi et al., 2011). The average annual rainfall is approximately 300 mm yr^{-1}, with a rainy season lasting from October to May. The rainfall patterns in this semi-arid area are highly variable in time and space. The temperature in Kairouan City ranges between a minimum of 10.7 °C in January and a maximum of 28.6 °C in August, with a mean value equal to 19.2 °C. The mean annual potential evapotranspiration (Penman) is close to 1600 mm. The landscape has no relief and land use is dominated by agriculture, with two main types of vegetation cover: annual agriculture and olive groves. A ground campaign carried out over different test fields revealed that the mean soil texture is composed of

HESSD
10, 8117–8144, 2013

45 % sand, 32 % clay and 23 % loam. Sandy soils are more commonly observed in the areas characterized by olive grove cultivation.

2.2 Satellite products

2.2.1 ERS/WSC moisture products

The scatterometers carried by ESA's dual ERS satellites[1] (launched in 1991 and 1995), are operated in the C-band (5.3 GHz) in the vertical polarization. Over land, the measured radar backscatter coefficient is sensitive to surface parameters (soil moisture, surface roughness, vegetation characteristics) and the emission characteristics of the radar (incidence angle, polarization and frequency). A change detection approach developed by the Institute of Photogrammetry and Remote Sensing (IPF), Vienna University of Technology (TU-Wien), has been used to estimate soil moisture from radar measurements (Wagner et al., 1999; Naeimi et al., 2008). The proposed moisture products have been validated in different regions of the globe, such as the Canadian Prairies (Wagner et al., 1999), the Iberian Peninsula (Ceballos et al., 2005), Western Africa (Wagner and Scipal, 2000; Zribi et al., 2008), and France (Paris Anguela et al., 2008). The TU-Wien algorithm is based on scaling of the normalized backscattering coefficient to a value corresponding to a 40° incidence angle, lying between the lowest value which occurs during the driest conditions, and the highest value which occurs during the wettest conditions. The retrieved moisture index, referred to as the "surface soil moisture" (ms), can range between 0 and 100 % and represents the water content present in the first 5 cm of soil. Based on the interpretation of cells approximately 50 km × 50 km in size, the proposed products have a grid spacing of 25 km, and a temporal resolution approximately two to three measurements per week. In order to compare ms values with ground measurements (Amri et al., 2012) or modeled surface moisture values, these products were converted to physical units of $m^3\,m^{-3}$, using the

[1] The dual ERS satellite mission was finally decommissioned in September 2011.

HESSD
10, 8117–8144, 2013

method described by (Pellarin et al., 2006). The Soil Water Index (SWI), which provides the water content along a profile 1 m in depth, is derived from the ms values measured on different successive dates. These products have already been validated and used in various hydrological studies (Ceballos et al., 2005; Pellarin et al., 2006; Paris Anguela et al., 2008).

2.2.2 SPOT-VGT NDVI products

The ten-day synthesis (S10) products derived from SPOT-VGT data are available at full resolution (1 km), and include 10 day NDVI data (Holben, 1986). For these products, top-of-atmospheric corrections have been applied. They use the SMAC algorithm (Rahman and Dedieu, 1994) which corrects molecular and aerosol scattering, water vapor, ozone and other gas absorption effects. The parameters taken into account in the atmospheric corrections are the aerosol optical depth (AOD), the atmospheric water vapor and ozone, together with a Digital Elevation Model used for atmospheric pressure estimation (Maisongrande et al., 2004). The water vapor parameter is obtained once every six hours from Météo-France. The AOD is retrieved from B0 band data combined with the NDVI (Maisongrande et al., 2004). Different systematic errors are corrected in the final *P* product, which is re-sampled to a Plate carrée geographic projection. The S10 products are available at http://free.vgt.vito.be.

2.3 Ground measurements

2.3.1 Precipitation data

Precipitation estimations for the studied site were based on a network of 30 rain gauges, distributed over the entire site (Fig. 2). The estimated precipitation levels were based on a network of rain gauges distributed over the entire site. The Inverse Distance Weighting (IDW) interpolation algorithm was used to derive daily precipitation maps. The IDW estimates values at non-sampled points, by computing the weighted

HESSD
10, 8117–8144, 2013

average of data observed at nearby points (Teegavarupu and Chandramouli, 2005; Shepard et al., 1968). The landscape is mainly flat in the validation areas, and there is no mountainous terrain able to influence the spatial distribution of rainfall. The precipitation time series and the NDVI data set are thus available with a spatial resolution of 1 km.

2.3.2 Meteorological data

Meteorological measurements, consisting of air temperature, humidity, wind speed, net radiation and rainfall measurements, were recorded over the last 20 yr by an automatic weather station. Daily averaged climatic parameters were calculated in order to determine the daily reference evapotranspiration ET_0 ($mm\,day^{-1}$), in accordance with the FAO-56 Penman-Monteith parameterization (Monteith, 1965).

The global radiation was determined from Météosat data retrieved from the SoDa server (Solar radiation Databases for environment, http://www.soda-is.com), established by the Mines ParisTech graduate school. In this database, global radiation data is available from January 1985 to December 2005, at temporal intervals of one day and a spatial resolution of 20 km.

2.4 Land use mapping

Low spatial resolution SPOT Vegetation NDVI images were used to map the land into three characteristic classes: olive trees, annual agriculture and pastures. It is important to note that these classes were labeled “Olives” and “Annual Agriculture”.

Remote sensing images typically contain a combination of pure and mixed pixels. These mixed pixels pose a difficult problem for land cover mapping, since their spectral characteristics are not representative of any single class of land cover, but rather of the combined signatures produced by more than one type of land cover present in each pixel.

HESSD
10, 8117–8144, 2013

In recent years, several approaches have focused on the disaggregation of low resolution mixed pixels in different land cover classes (Settle and Drake, 1993). In general, these authors consider information related to each class, retrieved from higher spatial resolution images or other ancillary products. A linear mixing theory is generally used, in which it is assumed that the reflectance (respectively NDVI) of a mixed pixel is given by the sum of the mean reflectance (respectively NDVI) values of the different land cover classes within the pixel, weighted by their corresponding fractional cover. The identification of typical NDVI profiles, representative of each of these land cover classes, is the first step in the disaggregation methodology. These pixels are identified by making use of information related to the class composition of each pixel, retrieved from a high-resolution land-cover map.

The general expression is given by Eq. (1), and the RMS of this quantity is given by Eq. (2):

$$\mathrm{Yi}(t) = \sum_{j=1}^{p} \pi_{ij} \times \rho j\,(t) + \varepsilon i(t) \tag{1}$$

$$\mathrm{RMSE}i = \sqrt{\frac{1}{T} \cdot \sum_{t=1}^{T} (\varepsilon i(t))} \tag{2}$$

where:

Yi(t) is the average signal observed at pixel i and at time t,
π_{ij} is the area occupied by the class j in pixel i
$\rho j(t)$ is the signal assigned to class j at time t,
εi is an error term,
p is the number of classes,
T is the number of observations,
i is the pixel index, and
j is the class index.

HESSD
10, 8117–8144, 2013

Disaggregation techniques try to estimate the proportion (between 0 and 1) of specific classes occurring within each pixel. The result is a certain number of fraction images, each corresponding to the relevant land-cover class. While this information describes the class composition, it does not provide any indication as to how the classes are spatially distributed within the pixel. The outcome is thus quite different from that obtained with conventional classification algorithms, in which a single "crisp" land cover map, containing all classes, is produced. Figure 3 shows a land use map for three classes.

3 Proposed model

3.1 Description of the basic FAO.56 model

The algorithm used in the present study is based on the FAO-56 dual crop coefficient model developed by (Allen, 1998), which describes the relationship between crop evapotranspiration under standard non-stressed conditions (ET_c) and a reference level of evapotranspiration (ET_0). The crop coefficient (K_c) is separated into two components: the basal crop coefficient (K_{cb}) and the soil water evaporation coefficient (K_e):

$$ET_C = (K_s \cdot K_{cb} + K_e) \cdot ET_0 \quad (3)$$

where ET_0 is estimated at 24 h intervals using the FAO Penman–Monteith equation.

The daily reference evapotranspiration ET_0 was determined with a spatial resolution of 20 km, allowing ET_0 maps to be derived at daily intervals, for each growing season from September to August, with the same resolution as the SoDa data. The cumulative annual ET_0 values are consistent with the levels observed in this region (approximately 1600 mm yr^{-1}).

HESSD
10, 8117–8144, 2013

3.2 Application with a dual vegetation cover

In the case of the present study, two types of vegetation cover are considered for each pixel: cereals and olive groves. For each pixel, the evapotranspiration is estimated as:

$$ET_C = \left[Fr_{cereals}\left[\left(f_{c-c}K_{cb-c} + \left(1 - f_{c-c}\right)K_e\right)\right] + Fr_{olive}\left[\left(f_{c-o}K_{cb-o} + \left(1 - f_{c-o}\right)K_e\right)\right]\right] \cdot ET_0 \quad (4)$$

The parameters (K_{cb} and K_e) used in Eq. (4) are derived from remotely sensed SPOT-VGT and ERS/WSC products.

3.2.1 Computation of K_{cb} and f_c values

Concerning annual agriculture (cereals), further details related to the proposed estimations can be found in (Er-raki et al., 2007). The calibrations made at the Tensift site in Morocco (Er-raki et al., 2007) was also used in for our studied site with high resemblance to Tensift. K_{cb} is defined as:

$$K_{cb} = 1.07 \cdot \left[1 - \left(\frac{NDVI - NDVI_{min}}{NDVI_{max} - NDVI_{min}}\right)^{\frac{0.84}{0.54}}\right] \quad (5)$$

where $NDVI_{min}$ and $NDVI_{max}$ are the minimum and maximum values of the NDVI, associated with bare soil and dense vegetation, respectively. The values used in the present study are 0.1 and 0.6.

f_c is the vegetation cover fraction defined by (Er-raki et al., 2007):

$$f_c = 1.18 \cdot (NDVI - NDVI_{min}) \quad (6)$$

In the case of olive groves, the crop coefficients proposed by the FAO in its Bulletin No. 56 (Allen et al., 1998) for the estimation of the water requirements of olive trees are not applicable to the present case study, due to the low percentage of this culture's

HESSD
10, 8117–8144, 2013

coverage. In a recent study, Testi et al. (2004) established a relationship between the ET and the cover fraction, which was used to determine the value of K_{cb} applicable to the present study.

In the case of olive groves, a tree spacing of approximately 20 m and a tree diameter of approximately 4 m area were considered. This leads to a value of fc value equal to 8 %.

3.2.2 Computation of the parameter K_e

In recent years, various different approaches have been proposed to relate soil resistance to soil moisture (Mahfouf and Noilhan, 1991; Chanzy and Bruckler, 1993; Simonneaux et al., 2009). Chanzy and Bruckler (1993) proposed an empirical method relating soil evaporation to soil moisture and climate demand, for different types of soil texture. In arid and semi-arid regions, the soil evaporation which occurs after a rainfall event is a process of major importance, whenever the local agriculture is characterized by a low density vegetation cover. An accurate estimation of this term thus allows a reliable estimation to be made of the stock of water available for use by the vegetation. In this section, a simple approach is used for the estimation of soil evaporation, which is equal to the ETP whenever the surface layer is saturated. A method developed by Merlin et al. (2011) was adapted, to allow soil evaporation to be related to the surface soil moisture (0–5 cm) estimated from radar satellite measurements. The K_e parameter can then be written as:

$$K_e = \left[\frac{1}{2} - \frac{1}{2}\cdot\cos\left(\pi\cdot\theta_L/\theta_{max}\right)\right]^P \quad \text{For } \theta_L \le \theta_{max} \tag{7}$$

where θ_L is the soil water content in the soil layer of thickness L, θ_{max} is the soil moisture at saturation, and P is a parameter given by the following expression.

$$P = \left(\frac{1}{2} + A_3\frac{L - L_1}{L_1}\right)\frac{LE_p}{B_3} \tag{8}$$

HESSD
10, 8117–8144, 2013

In this expression, $L1$ is the thinnest layer of soil represented (here 0–5 cm), and $A3$ (unit-less) and $B3$ ($W m^{-2}$) are the two a priori best-fit parameters, which depend on the soil's texture and structure.

θ_{max} was estimated from continuous ground thetaprobe measurements, acquired over a period of three years. The soil evaporation is assumed to be at its maximum for saturated soils, with a value defined as being equal to ET_0, which is close to zero for very dry surfaces.

4 Validation of the FAO model

4.1 Description of the ISBA model

The ISBA model applies the force-restor method proposed by Deardoff (1978) to compute the corresponding variations in soil surface energy and water budget (Noilhan and Planton, 1989). Three layers are used to represent the soil hydrology, an upper surface layer, a root-zone layer and a deep soil layer (Boone et al., 1999). Water interception storage and snow pack variations are also taken into account in the ISBA model (Douville et al., 1995). Within each grid, the ISBA model takes the heterogeneity of infiltration, precipitation, topography and vegetation into account. The conversion of precipitation into runoff over saturated surfaces is based on the TOPMODE approach (Beven and Kirkby, 1979; Decharme et al., 2006). Within each grid cell, the heterogeneity of land cover and soil depths is taken into account through the use of a tile approach, in which the cell is divided into a series of sub-grid patches. For each tile in a grid cell, distinct energy and water budgets are calculated. The multiplicative model developed by Jarvis (1976) is used to determine the stomatal resistance of the vegetation. The ECOCLIMAP look-up tables are used to generate the LAI (Leaf Area Index) inputs used by the ISBA model.

ISBA-A-gs corresponds to a variant of the ISBA model (Calvet et al., 1998), which takes photosynthesis and its coupling with leaf-level stomatal conductance into

HESSD
10, 8117–8144, 2013

account, and in which a biochemical soil–vegetation–atmosphere transfer representation is used for the photosynthesis model (Arora, 2002). ISBA-A-gs also implements a new representation for soil moisture stress, with which two different drought responses can be applied: one is used for herbaceous vegetation (Calvet, 2000), and the other for forests (Calvet et al., 2004).

4.2 Validation of the ISBA soil moisture output

Figure 4 illustrates a comparison between ERS/WSC soil moistures, ISBA output and precipitation time series. Three statistical parameters (the root mean square error (RMSE), the coefficient of determination (R^2), and the bias) are considered for the evaluation of comparison between the ERS and ISBA data sets.

The satellite data products were compared with two ISBA outputs; the modeled top layer (the first five centimeters of soil) and the soil moisture profiles (down to a depth of 100 cm), for the 16 yr period from 1991 to 2007. As can be seen in Fig. 4, local variations in the ERS surface products are not completely retrieved by the ISBA outputs. In fact, the latter corresponds to the first ten centimeters of soil, which are less affected by atmospheric conditions (rain, wind and solar radiation) than the first two or three centimeters of soil measured by the ERS/WSC radar. Despite the strong heterogeneity of the moisture profile in the first centimeters, the statistics of the resulting comparison are good: RMSE = 0.04 $m^3 m^{-3}$, bias = 0.02, and R^2 = 0.52.

In Fig. 4b, the monthly SWI ISBA outputs (0.5 m depth) are compared with the ERS estimations, showing that these two products have a good degree of coherence. In general, a delay of several days is observed between significant rainfall events and the corresponding increase in water soil content, determined using the ERS measurements. The statistics of the compared data are good: RMSE equal to 0.03 $m^3 m^{-3}$, R^2 = 0.5, and a low bias, equal to 0.008.

HESSD
10, 8117–8144, 2013

4.3 Validation of the evapotranspiration output produced by the FAO model

Figure 5 compares the ISBA and FAO model evapotranspiration simulations over the studied area, for a single ISBA pixel (0.5° × 0.5°) during (1998–2000 and 2004–2005). The two products were compared only on dates for which ERS/WSC measurements were recorded, to ensure that satellite measurements of the K_e evaporation parameter could be applied. The two products are found to be in good agreement, and the statistical parameters derived from the simulation are reasonable: RMSE equal to 0.36 mm day^{-1}, with a correlation strength given by $R^2 = 0.55$.

Figure 6a compares the evapotranspiration simulated by the ISBA-A-gs model with that predicted by the FAO-56 model, for the 1998–1999 agricultural season, during which the total precipitation was approximately 280 mm. A good degree of consistency is observed for the results obtained with these two models. However, it can be seen that on some dates, the simulated evapotranspiration is underestimated, probably as a consequence of the rainfall events taken into account in the ISBA-A-gs model. The statistical parameters derived from the simulation are reasonable: RMSE equal to 0.39 mm day^{-1}, correlation strength given by $R^2 = 0.55$, and a low bias equal to 0.009 mm day^{-1}.

The second example, illustrated in Fig. 6b, corresponds to the 1999–2000 agricultural season, characterized by a relatively dry growing season and a total annual precipitation of approximately 250 mm. During this season, the results given by the two models are found to be more consistent. The FAO-56 model retrieves almost the same trends as the ISBA-A-gs model, for both high and low values of evapotranspiration. The statistical parameters from the comparison are good: RMSE = 0.25 mm day^{-1}, correlation strength $R^2 = 0.61$, and a low bias equal to 0.01. For both of these agricultural seasons, the two models are found to be well correlated with the rainfall events, with a clear increase in the level of evapotranspiration following strong precipitation events. However, some distinct inconsistencies can be observed between the two simulations. As an example, in April 1999 the FAO-56 model retrieves a high level of evapotranspiration,

HESSD
10, 8117–8144, 2013

due to a 10 mm precipitation event, which was not detected by the ISBA-A-gs simulations. Conversely, in May 2000 a rise is observed in the level of evapotranspiration predicted by the ISBA-A-gs model, which is not predicted by the FAO-56 model. Prior to this peak in the ISBA-A-gs model, one small (1 mm) rainfall event occurred, which probably had a very limited influence on the real level of evapotranspiration. It is thus likely that the discrepancy observed between the two models results from an exaggeration of this event, at the precipitation input of the ISBA-A-gs model.

Finally, the seasonal cumulative water requirement maps for the 1998–1999, 1999–2000 and 2004–2005 agricultural seasons, estimated by the FAO-56 dual crop coefficient model combined with satellite data, are shown in Fig. 7. It should be noted that these maps are compatible with the land use maps. As an example, for the 1998–1999 agricultural year the water requirements were slightly greater for annual crops (400 mm) than for olive groves (200 mm).

By comparing the water requirements of annual crops with the average annual rainfall in the Kairouan plain (300 mm) an initial estimation of the hydric deficit, which can be offset through the use of irrigation, is achieved.

5 Conclusions

A dual FAO-56 model is proposed for the simulation of evapotranspiration at regional scales. This is combined with remotely sensed, multi-sensor data. Two main types of vegetation cover, cereals and olive trees, are considered in this analysis. The vegetation fractions represented by these two classes are retrieved by means of a multi-temporal classification of SPOT-VGT time series images. The evapotranspiration is computed over the studied area for two vegetation classes, weighted by their respective vegetation fractions.

The cereal crop coefficient and vegetation fraction estimations were based on NDVI-SPOT vegetation data, through the use of an empirical relationship. Soil evaporation was estimated by a simple approach developed by Merlin et al. (2011), established

HESSD
10, 8117–8144, 2013

between this quantity and surface soil moisture, using ERS/WSC radar products developed by the University of Vienna. Saturated soils are associated with the highest level of evaporation, and the driest soils have approximately zero evaporation.

The ISBA-A-gs SVAT model was used to validate the FAO approach, using simulations covering the period between 1991 and 2007. The ISBA soil moisture outputs were validated using ERS/WSC products developed by the University of Vienna. A good degree of coherence is observed for surface moisture, with an RMSE equal to 0.04 $m^3 m^{-3}$, R^2 equal to 0.52 and a bias equal to 0.002. The soil moisture profiles are also in good agreement, with an RMSE equal to 0.03 $m^3 m^{-3}$, R^2 equal to 0.5, and a bias equal to 0.008. A comparison between the results produced by the ISBA and FAO models, for the same study area, shows that they are strongly coherent. In the case of daily comparisons, an RMSE equal to 0.36 mm day^{-1} is found, which is low by comparison with the mean ET values, estimated at approximately 2 mm day^{-1}. The soil moisture profiles have a good correlation, with R^2 equal to 0.5. These results illustrate the strong potential of this simple approach, in which the FAO-56 model is combined with satellite observations, to retrieve evapotranspiration levels in semi-arid regions.

Acknowledgements. This study was funded by two sources: the French national MISTRALS program, and the French Institut de Recherche pour le Développement (Institute for Research and Development). The authors extend their thanks to VITO for kindly providing them with its SPOT-VEGETATION NDVI products, and to the ISIS program for providing them with the SPOT images used in this study. They would also like to thank the Tunisian Ministry of Agriculture for providing the precipitation data used in this study, as well as the technical teams of the IRD, INAT, CTV-Chebika and INGC for their strong collaboration and support with the implementation of ground-truth measurements.

The publication of this article
is financed by CNRS-INSU.

HESSD
10, 8117–8144, 2013

References

Allen, R. G.: Using the FAO-56 dual crop coefficient method over an irrigated region as part of an evapotranspiration intercomparison study, J. Hydrol., 229, 27–41, 2000.

Allen, R. G., Pereira, L. S., Raes, D., and Smith, M.: Crop Evapotranspiration-Guidelines for Computing Crop Water Requirements, Irrigation and Drain, Paper No. 56, FAO, Rome, Italy, 300 pp., 1998.

Amri, R., Zribi, M., Lili-Chabaane, Z., Wagner, W., Hauesne, S.: Analysis of ASCAT-C band scatterometer estimations derived over a semi-arid region, IEEE T. Geosci. Remote, 50, Part I, 2630–2638, 2012.

Arora, V. K.: Modeling vegetation as a dynamic component in soil-vegetationatmosphere transfer schemes and hydrological models, Rev. Geophys., 40, 1006, doi:10.1029/2001RG000103, 2002.

Beven, K. and Kirkby, M. J.: A physically based variable contributing area model of basin hydrology, Hydrol. Sci. Bull., 24, 43–69, 1979.

Boone, A., Calvet, J.-C., and Noilhan, J.: Inclusion of a third soil layer in a land surface scheme using the force restore method, J. Appl. Meteorol. 38, 1611–1630, 1999.

Braud, I., Dantas Antonio, A. C., Vauclin, M., Thony, J. L., and Ruelle, P.: A Simple Soil Plant Atmosphere Transfer model (SisPAT): Development and field verification, J. Hydrol., 166, 213–250, 1995.

Calvet, J.-C.: Investigating soil and atmospheric plant water stress using physiological and micrometeorological data, Agr. For. Meteorol., 103, 229–247, 2000.

Calvet, J. C., Noilhan, J., Roujean, J. L., Bessemoulin, P., Cabelguenne, M., Alioso, A. and Wigneron, J. P.: An interactive vegetation SVAT model tested against data from six contrasting sites, Agr. For. Meteorol., 92, 92–95, 1998.

Calvet, J.-C., Rivalland, V., Picon-Cochard, C., Guehl, J.-M.: Modelling forest transpiration and CO_2 fluxes – response to soil moisture stress, Agr. For. Meteorol., 124, 143–156, 2004.

Ceballos, A., Scipal, K., Wagner, W., and Martinez-Fernandez, J.: Validation of ERS scatterometer-derived soil moisture data in the central part of the Duero Basin, Spain, Hydrol. Process., 19, 1549–1566, 2005.

Chanzy, A. and Bruckler, L.: Significance of soil surface moisture with respect to daily bare soil evaporation, Water Resour. Res., 29, 1113–1125, 1993.

HESSD
10, 8117–8144, 2013

Coudert, B., Ottlé, C., Boudevillain, B., Demarty, J., and Guillevic, P.: Contribution of thermal infrared remote sensing data in multiobjective calibration of a dual-source SVAT model, J. Hydrometeorol., 7, 404–420, 2006.
Deardorff, J. W.: Efficient prediction of ground surface temperature and moisture, with inclusion of a layer of vegetation, J. Geophys. Res., 83, 1889–1903, 1978.
Deblonde, G. and Cihlar, J.: A multiyear analysis of the relationship between surface environmental variables and NDVI over the Canadian landmass, Remote Sens. Rev., 7, 151–177, 1993.
Decharme, B., Douville, H., Boone, A., Habets, F., Noilhan, J.: Impact of an exponential profile of saturated hydraulic conductivity within the ISBA LSM: simulations over the Rhône basin, J. Hydrometeorol., 7, 61–80, 2006.
Douville, H., Royer, J.-F., Mahfouf, J.-F.: A new snow parameterization for the Meteo-France climate model, Part 1: validation in stand-alone experiments, Clim. Dynam., 12, 21–35, 1995.
Duchemin, B., Hadria, R., Er-Raki, S., Boulet, G., Maisongrande, P., Chehbouni, A., Escadafal, R., Ezzahar, J., Hoedjes, J., Karrou, H., Khabba, S., Mougenot, B., Olioso, A., Rodriguez, J.-C., and Simonneaux, V.: Monitoring wheat phenology and irrigation in Central Morocco: on the use of relationship between evapotranspiration, crops coefficients, leaf area index and remotely-sensed vegetation indices, Agr. Water Manage., 79, 1–27, 2006.
Er-Raki, S., Chehbouni, G., Guemouria, N., Duchemin, B., Ezzahar, J., Hadria, R.: Combining FAO-56 model and ground-based remote sensing to estimate water consumptions of wheat crops in a semi-arid region, Agr. Water Manage., 87, 41–54, 2007.
Er-Raki, S., Chehbouni, A., Boulet, G., and Williams, D. G.: Using the dual approach of FAO-56 for partitioning ET into soil and plant components for olive orchards in a semi-arid region, Agr. Water Manage., 97, 1769–1778, 2010.
Fraser, R. S. and Kaufman, Y. J.: The relative importance of scattering and absorption in remote sensing, IEEE Trans. Geosci. Remote Sens. 23, 625–633, 1985.
Holben, B. N., Kaufaman, Y. J., Kendall, J. D.: NOAA-11 AVHRR visible and near-IR inflight calibration, Int. J. Remote Sens, 11, 1511–1519, 1990.
Jackson, T. J., Schmugge, J., and Engman, E. T.: Remote sensing applications to hydrology: soil moisture, Hydrolog. Sci. J., 41, 517–530, 1996.
Jarvis, P. G.: The interpretation of the variations in the leaf water potential and stomatal conductance found in canopies in the field, Philos. T. R. Soc. London, 273, 593–610, 1976.

HESSD
10, 8117–8144, 2013

Laurila, H., Karjalainen, M., Kleemola, J., and Hyyppä, J.: Cereal yield modeling in Finland using optical and radar remote sensing, Remote Sens., 2, 2185–2239, 2010.
Mahfouf, J. F. and Noilhan, J.: Comparative study of various formulations of evaporation from bare soil using in situ data, J. Appl. Meteorol. Clim, 30, 1354–1365, 1991.
Mahfouf, J.-F., Manzi, O., Noilhan, J., Giordani, H., and Déqué, M.: The land surface scheme ISBA within the Météo-France climate model ARPEGE, Part I: Implementation and preliminary results, J. Climate, 8, 2039–2057, 1995.
Maisongrande, P., Duchemin, B., and Dedieu, G.: VEGETATION/SPOT: an operational mission for the Earth monitoring, presentation of new standard products, Inter J. Remote Sens., 25, 9–14, 2004.
Merlin, O., Al Bitar, A., Rivalland, V., Beziat, P., Ceschia, E., Dedieu, G.: An analytical model of evaporation efficiency for unsaturated soil surfaces with an arbitrary thickness, J. Appl. Meteorol. Clim., 50, 457–471, 2011.
Monteith, J. L. Evaporation and environment: the state and movement of water in living organisms, Symp. Soc. Exp. Biol., 19, 205–234, 1965.
Myneni, R. B., Los, S. O., and Asrar, G.: Potential gross primary productivity of terrestrial vegetation from 1982 to 1990, Geophyis. Res. Lett., 22, 2617–2620, 1995.
Naeimi, V., Bartalis, Z., and Wagner, W.: ASCAT soil moisture: An assessment of the data quality and consistency with the ERS scatterometer heritage, J. Hydrometeorol., 10, 555–563, doi:10.1175/2008JHM1051.1, 2008.
Noilhan, J. and Planton, S.: A simple parameterization of land surface processes for meteorological models, Mon. Weather Rev., 117, 536–549, 1989.
Paris Anguela, T., Zribi, M., Hasenauer, S., Habets, F., and Loumagne, C.: Analysis of surface and root-zone soil moisture dynamics with ERS scatterometer and the hydrometeorological model SAFRAN-ISBA-MODCOU at Grand Morin watershed (France), Hydrol. Earth Syst. Sci., 12, 1415–1424, doi:10.5194/hess-12-1415-2008, 2008.
Pellarin, T., Calvet, J. C., and Wagner, W.: Evaluation of ERS scatterometer soil moisture products over a half-degree region in southwestern France. Geophys. Res. Lett., 33, L17401, doi:10.1029/2006GL027231, 2006.
Propastin, P. and Kappas, M.: Modeling net ecosystem exchange for grassland in Central Kazakhstan by combining remote sensing and field data, Remote Sens., 1, 159–183, 2009.

HESSD
10, 8117–8144, 2013

Purevdorj, T., Tateishi, R., Ishiyama, T., and Honda, Y.: Relationships between percent vegetation cover and vegetation indices, Int, J. Remote Sens., 19, 3519–3535, 1998.
Rahman, H. and Dedieu, G.: SMAC: a simplified method for the atmospheric correction of satellite measurements in the solar spectrum, Int, J. Remote Sens., 15, 123–143, 1994.
Sellers, P. J.: Canopy reflectance, photosynthesis and transpiration, Int, J. Remote Sens., 6, 1335–1372, 1985.
Settle, J. J. and Drake, N. A.: Linear mixing and the estimation of ground cover proportions, Int, J. Remote Sens., 14, 1159–1177, 1993.
Shepard, D.: A two dimensional interpolation function for regularly spaced data, in: Proceedings of National Conference of the Association for Computing Machinery, Princeton, NJ, USA, 517–524, 1968.
Simonneaux, V., Lepage, M., Helson, D., Metral, J., Thomas, S., Duchemin, B., Cherkaoui, M., Kharrou, H., Berjami, B., and Chehbouni, A.: Estimation spatialisée de l'évapotranspiration des cultures irriguées par télédétection: application à la gestion de l'irrigation dans la plaine du Haouz (Marrakech, Maroc), Sècheresse, 20, 123–130, 2009
SPOT Vegetation User's Guide: available at: http://www.vgt.vito.be/userguide/userguide.htm (last access: 18 November 2011), 2008.
Testi, L., Villalobos, F. J., and Orgaz, F.: Evapotranspiration of a young irrigated olive orchard in southern Spain, Agr. For. Meteorol., 121, 1–18, 2004.
Teegavarapu, R. and Chandramouli, V.: Improved weighting methods, deterministic and stochastic data-driven models for estimation of missing precipitation records, J. Hydrol., 312, 191–206, 2005.
Ulaby, F. T., Dubois, P. C., and van Zyl, J.: Radar mapping of surface soil moisture, J. Hydrol., 184, 57–84, 1996.
Wagner, W. and Scipal, K.: Large-scale soil moisture mapping in western Africa using the ERS scatterometer, IEEE T.. Geosci. Remote Sens., 38, 1777–1782, doi:10.1109/36.851761, 2000
Wagner, W., Noll, J., Borgeaud, M., and Rott, H.: Monitoring soil moisture over the Canadian prairies with the ERS scatterometer, IEEE Geosci. Remote Sens., 37, 206–216, 1999.
Zribi, M., Le Hegarat-Mascle, S., Ottlé, C., Kammoun, B., and Guerin, C.: Surface soil moisture estimation from the synergistic use of the (multi-incidence and multi-resolution) active microwave ERS Wind Scatterometer and SAR data, Remote Sens. Environ., 86, 30–41, 2003.

HESSD
10, 8117–8144, 2013

Zribi, M., André, C., and Decharme, B.: A method for soil moisture estimation in Western Africa based on the ERS scatterometer, IEEE Trans. Geosci. Remote Sens, 46, 438–448, doi:10.1109/TGRS.2007.904582, 2008.

Zribi, M., Chahbi, A., Shabou, M., Lili-Chabaane, Z., Duchemin, B., Baghdadi, N., Amri, R., and Chehbouni, A.: Soil surface moisture estimation over a semi-arid region using ENVISAT ASAR radar data for soil evaporation evaluation, Hydrol. Earth Syst. Sci., 15, 345–358, doi:10.5194/hess-15-345-2011, 2011.

HESSD

10, 8117–8144, 2013

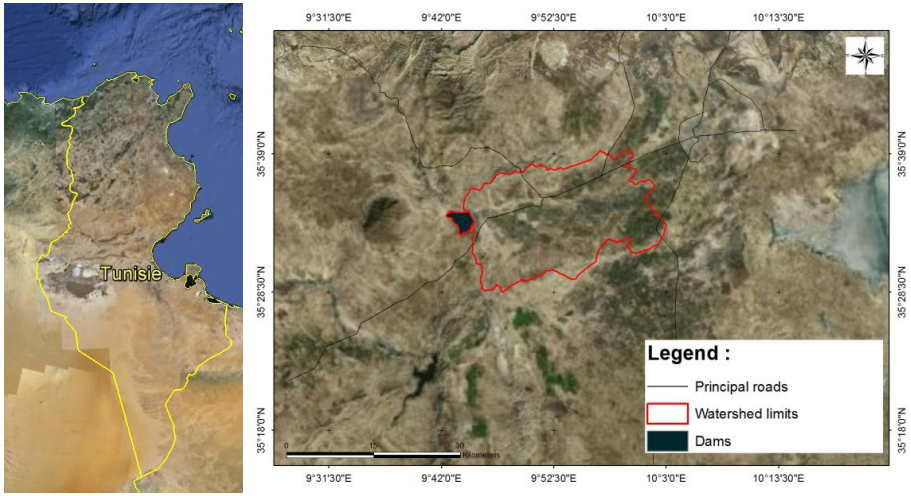

Fig. 1. Illustration of the studied area.

HESSD
10, 8117–8144, 2013

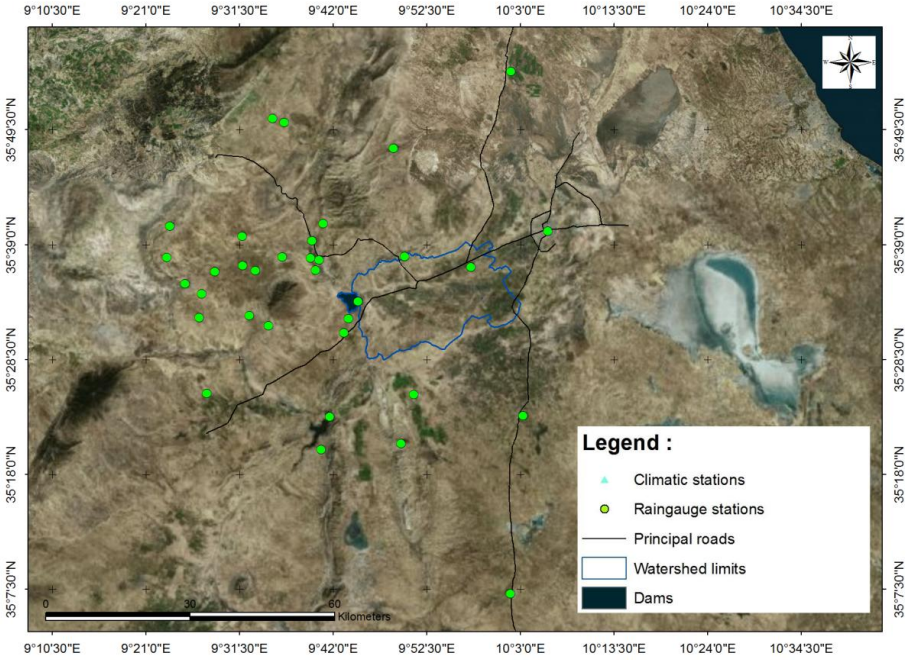

Fig. 2. Network of rainfall and climate stations present on the Kairouan plain.

HESSD
10, 8117–8144, 2013

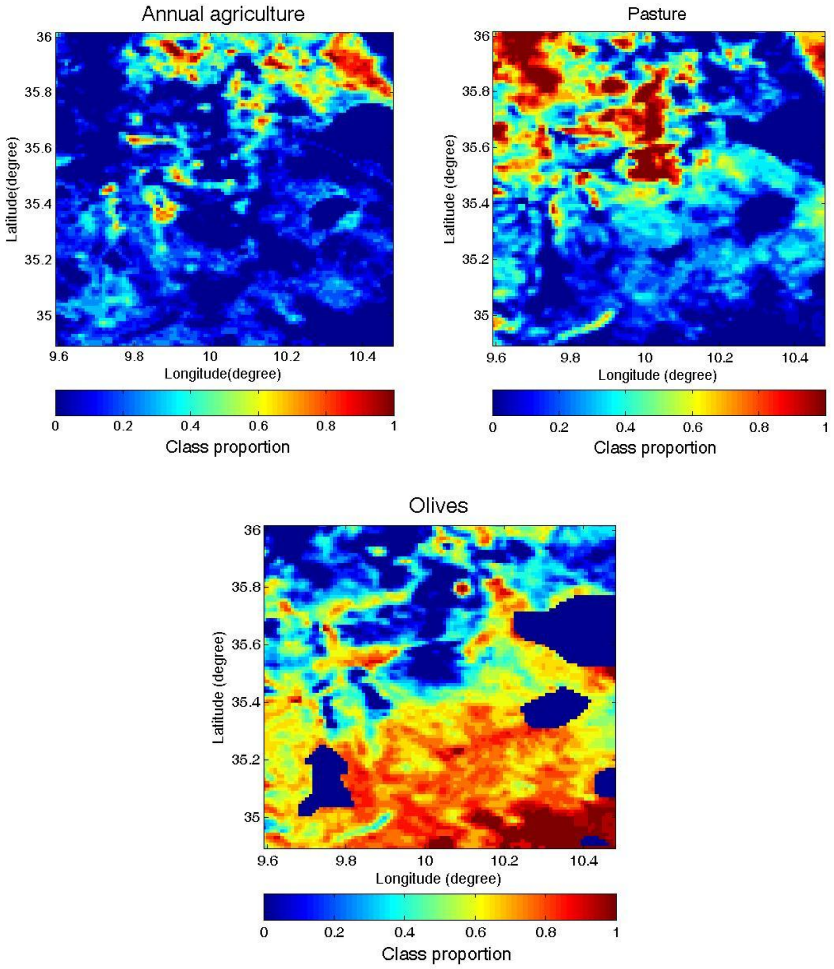

Fig. 3. Land use map for the 2008–2009 agricultural season.

HESSD
10, 8117–8144, 2013

FAO-56 dual approach combined with multi-sensor remote sensing

R. Amri et al.

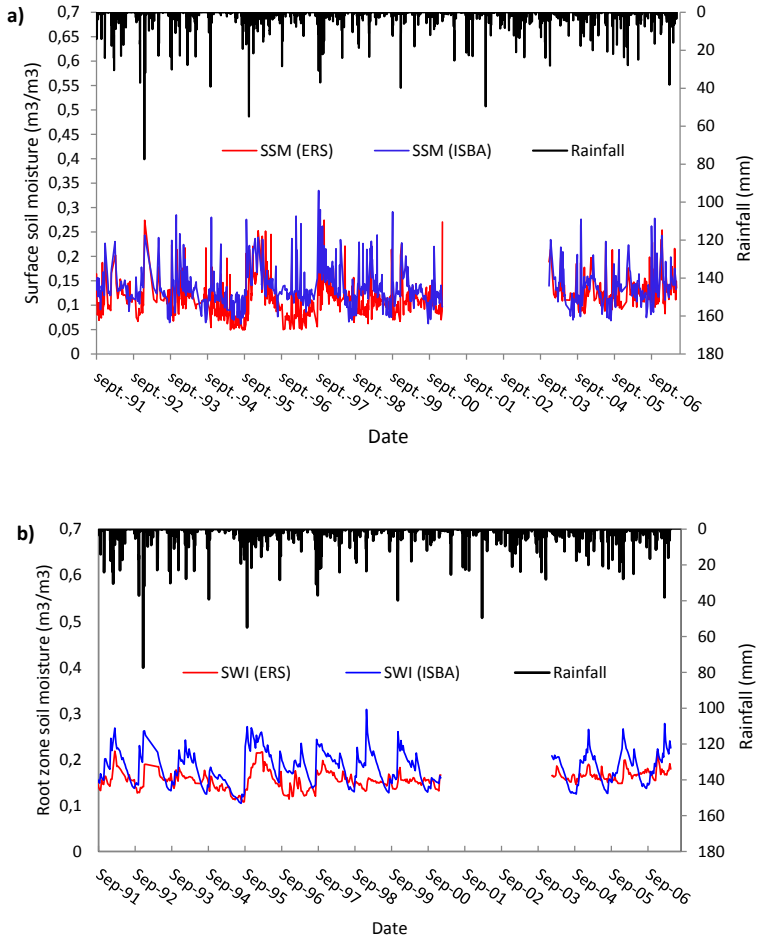

Fig. 4. Inter-comparison between ISBA-A-gs soil moisture outputs and ERS/WSC products, **(a)** surface soil moisture, **(b)** root zone moisture.

HESSD
10, 8117–8144, 2013

FAO-56 dual approach combined with multi-sensor remote sensing

R. Amri et al.

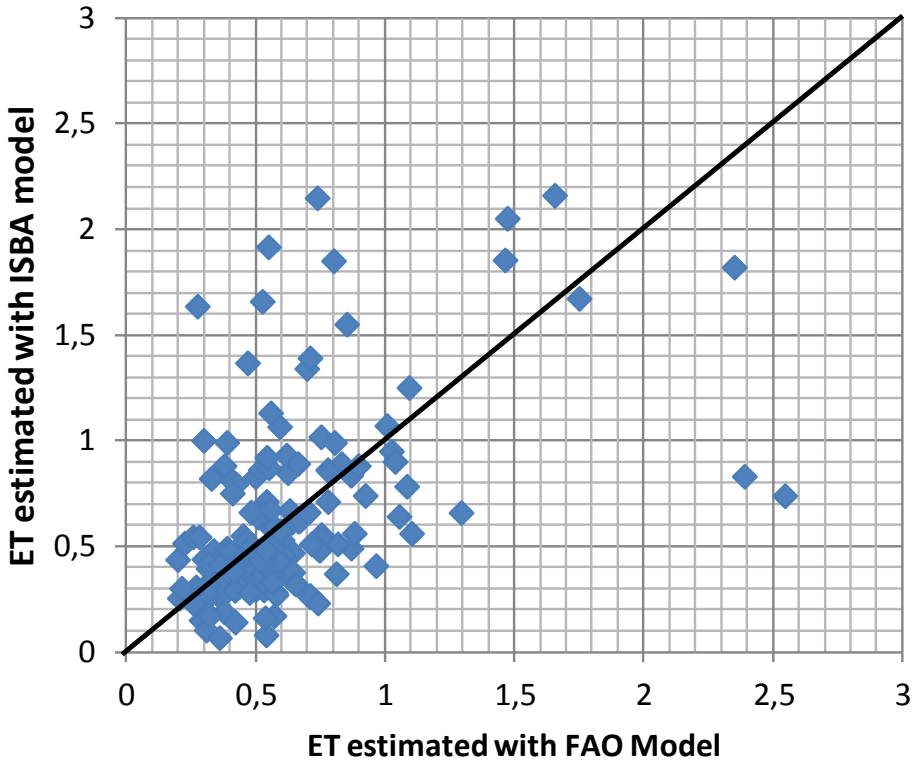

Fig. 5. Evapotranspiration simulated by the ISBA-A-gs model, as a function of the levels simulated by the FAO-56 model.

HESSD
10, 8117–8144, 2013

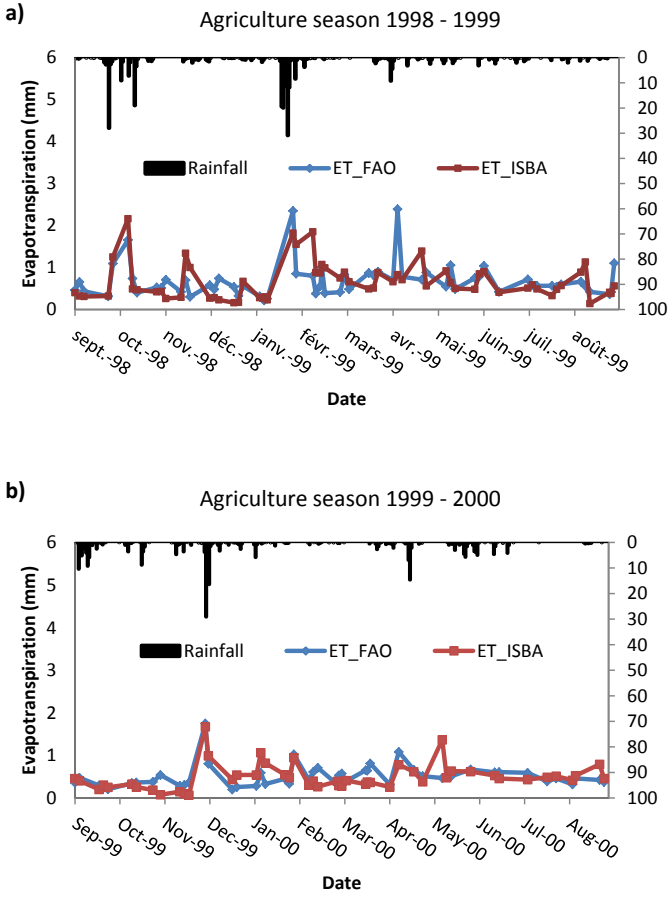

Fig. 6. Intercomparison evapotranspiration outputs of the two models FAO-56 and ISBA-A-gs: **(a)** agricultural season 1998–1999; **(b)** agricultural season 1999–2000.

HESSD
10, 8117–8144, 2013

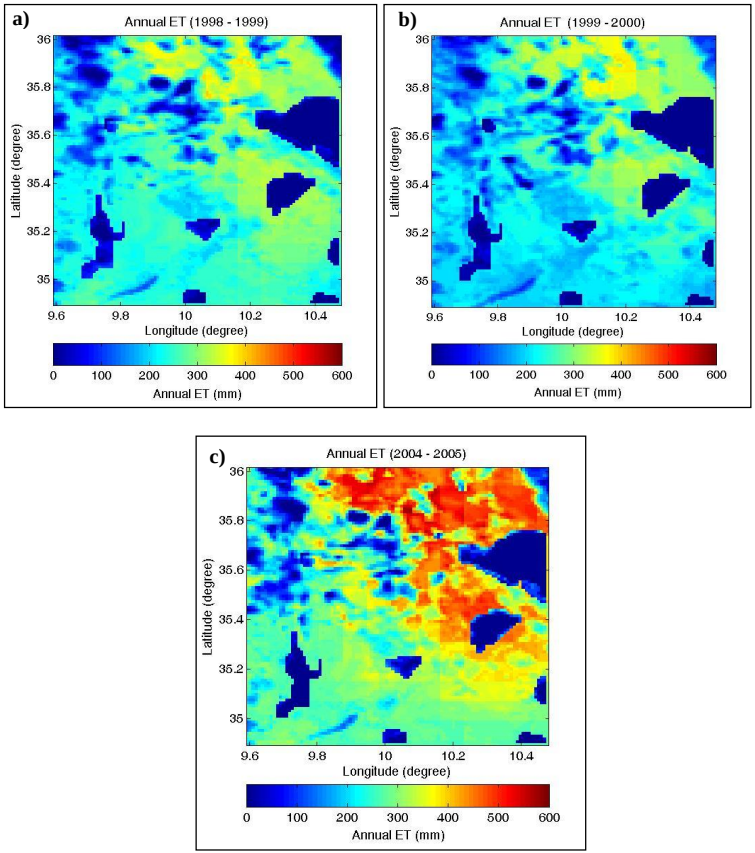

Fig. 7. Total annual evapotranspiration maps: **(a)** 1998–1999 agricultural season; **(b)** 1999–2000 agricultural season **(c)** 2004–2005 agricultural season.

HESSD
10, 8117–8144, 2013